chinaXiv:202212.00178v3

Ultra-low-noise transimpedance amplifier with a single HEMT in pre-amplifier for measuring shot noise in cryogenic STM

Ying-Xin Liang*
Anyang Normal Univ, Sch Phys & Elect Engn, No.436, Xiange Avenue, Anyang 455000, Henan, China

December 27, 2022

Abstract

In this work, a design of transimpedance amplifier (TIA) for cryogenic scanning tunneling microscope (CryoSTM) is proposed. The TIA with the tip-sample component in CryoSTM is called as CryoSTM-TIA. With transimpedance gain of 1 GΩ, the bandwidth of the CryoSTM-TIA is larger than 300 kHz. The distinctive feature of the proposed CryoSTM-TIA is that its pre-amplifier is made of a single cryogenic high electron mobility transistor (HEMT), so the apparatus equivalent input noise current power spectral density at 100 kHz is lower than 4 $(\text{fA})^2/\text{Hz}$. In addition, "bias-cooling method" can be used to in-situ control the density of the frozen DX^- centers in the HEMT doping area, changing its structure to reduce the device noises. With this apparatus, fast scanning tunneling spectra measurements with high-energy-resolution are capable to be performed. And, it is capable to measure scanning tunneling shot noise spectra (STSNS) at the atomic scale for various quantum systems, even if the shot noise is very low. It provides a powerful tool to investigate novel quantum states by measuring STSNS, such as detecting the existence of Majorana bound states in the topological quantum systems.

1 Introduction

High performance transimpedance amplifier (TIA) for cryogenic scanning tunneling microscope (CryoSTM) is a key element [1, 2]. Recently, in Ref.[3], it was proposed a design of TIA for CryoSTM. The TIA with the tip-sample component in CryoSTM is called as CryoSTM-TIA. In that design, the CryoSTM-TIA has a transimpedance gain of 1 GΩ, a bandwidth of more than 300 kHz, and its equivalent input noise current power spectral density (PSD) that characterizes the circuit inherent noise is 21 $(\text{fA})^2/\text{Hz}$ at 100 kHz. The CryoSTM-TIA is capable of measuring the scanning tunneling shot noise spectra (STSNS) of various quantum systems at atomic resolution, even if the measured noise current PSD is as small as a few $(\text{fA})^2/\text{Hz}$. In Ref.[3], it was illustrated how the CryoSTM-TIA is used to measure STSNS of quantum systems to investigate novel quantum states, such

*E-mail address: cryoliang@qq.com

chinaXiv:202212.00178v3

as detecting Majorana bound states (MBSs) in iron-based superconductors [4]. In the CryoSTM-TIA, cascade the pre-amplifier (Pre-Amp) and the post-amplifier (Post-Amp) to form an operational amplifier (OPA), and denoted as Macro-Amp. The Pre-Amp in the Macro-Amp is a differential amplifier made of a pair of high electron mobility transistors (HEMTs), where the HEMT is a kind of cryogenic GaAs MESFET [5, 6]. However, it is quite difficult to select cryogenic GaAs MESFETs with identical performances for pairing [2].

In this work, a design for the CryoSTM-TIA with a single HEMT in the Pre-Amp is proposed. In the CryoSTM-TIA, cascade Pre-Amp and Post-Amp to form an inverting-amplifier (Inv-Amp), which is not OPA. The CryoSTM-TIA still has transimpedance gain of 1GΩ and bandwidth more than 300 kHz. However, its equivalent input noise current PSD is only 3 $(\text{fA})^2/\text{Hz}$ at 100 kHz, i.e. 1/7 of that in Ref.[3], since a noisy HEMT is reduced. Therefore, the lower tunneling shot noise of quantum systems can be measured at the atomic scale with this apparatus. Furthermore, only a single HEMT is used in the Pre-Amp, avoiding the difficulty of matching two identical HEMTs. And, "bias-cooling method" [5] can be used to in-situ reduce the inherent noise of the HEMT. With these advantages, this apparatus will be a powerful tool to investigate novel quantum states in various quantum systems, in the wider range of applications than that in Ref.[3], such as high-T_c superconductors [7, 8], topological superconductors [4], MBSs [4, 9, 10, 11, 12], Andreev reflection [13, 14], and Kondo effect [15], etc.

2 Circuit of the proposed CryoSTM-TIA

The circuit of the proposed CryoSTM-TIA is shown in Fig.1. It consists of several components: the single HEMT amplifier part of the Pre-Amp shown in dashed box (a1) of Fig.1, the constant-current source part of the Pre-Amp in dashed box (a2), the post-amplifier (Post-Amp) shown in dashed box (b), the compensated feedback network shown in dashed box (c), and the signal source circuit shown in dashed box (d). The two stage amplifier made of the Pre-Amp and the Post-Amp is called as inverting-amplifier (Inv-Amp). The Inv-Amp is connected with the feedback network to form the TIA. The input G of the TIA is connected to the signal source circuit, to form the CryoSTM-TIA. The components placed in the cryogenic zone are shown in the dotted box. The parameters of all components of the CryoSTM-TIA circuit are listed in Table 1.

2.1 Design of Pre-Amp

As shown in Fig.1, only a single cryogenic HEMT is used in the Pre-Amp. The HEMT in this work is CNRS-HEMT (denoted as C-H) [5, 6] developed by CNRS/LPN in France with the excellent cryogenic and noise characteristics. It is capable of operating under 0.5 K with only 0.1 mW on the ideal operating point of "$V_{\text{ds}} = 100$ mV and $I_{\text{ds}} = 1$ mA". Its parameters are listed in Table 1, where $\overline{e_{\text{H}}^2}$ is its equivalent input noise voltage PSD and $\overline{i_{\text{H}}^2}$ is its equivalent input noise current PSD [6].

The single HEMT amplifier part of the Pre-Amp is shown in dashed box (a1) in Fig.1. The source of C-H is grounded by a resistor R_{s} and a small variable resistor R_{s1}. $R_{\text{S}} = R_{\text{s}} + R_{\text{s1}}$, and a capacitor C_{S} of 0.1 mF is in parallel with R_{S}. Drain O_1 of C-H is connected to the load resistor R_1, and L_1 as the other end of R_1 is connected to output P

chinaXiv:202212.00178v3

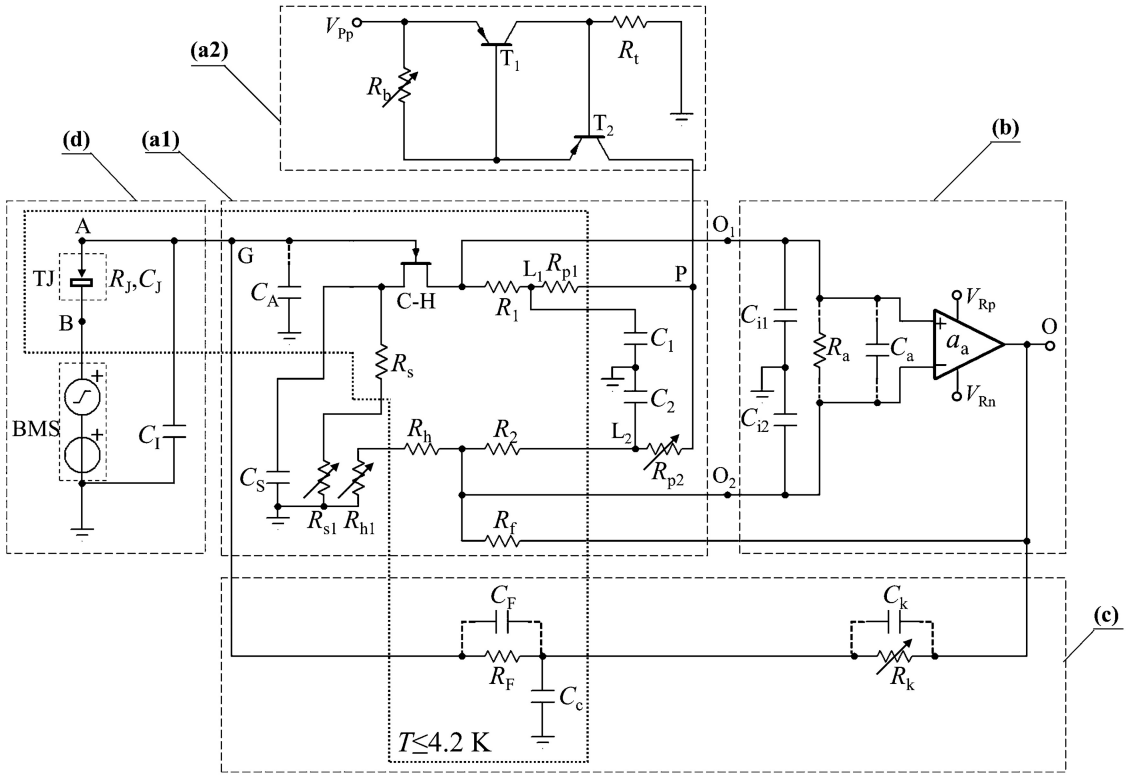

Figure 1: Circuit of the proposed CryoSTM-TIA. Single HEMT amplifier part of Pre-Amp is shown in dashed box (a1), constant-current source part of Pre-Amp in dashed box (a2), Post-Amp in dashed box (b), compensated feedback network in dashed box (c), and signal source circuit in dashed box (d). The components placed in the cryogenic zone are shown in the dotted box. The parameters of all components of CryoSTM-TIA circuit are listed in Table 1.

of the constant-current source through a small resistor $R_{\rm p1}$. The resistor $R_{\rm h}$ is grounded through the variable resistor $R_{\rm h1}$. $R_{\rm H} = R_{\rm h} + R_{\rm h1}$. The other end of $R_{\rm h}$, denoted as $\rm O_2$, is connected to the resistors R_2, and $\rm L_2$ as the other end of R_2 is connected to P through a small variable resistor $R_{\rm p2}$. $R_1 = R_2 = R_{\rm L}$. $\rm L_1$ and $\rm L_2$ are grounded by the capacitors C_1 and C_2 respectively, and $C_1 = C_2 = C_{\rm L}$ =10 μF. $C_{\rm A}$ is the input capacitance of the Pre-Amp. C-H, $R_{\rm s}$, $R_{\rm h}$, R_1, R_2, and $R_{\rm p1}$ are placed in the cryogenic zone, shown in the dotted box. $C_{\rm I}$ is the capacitance of the cable that connects gate G of C-H and the tip in the CryoSTM. C-H is as close to the tip as possible to reduce $C_{\rm I}$, which can be less than 0.5 pF. The operating point adjustment for the Pre-Amp is shown in Sect.4. The Pre-Amp parameters are shown in Table 1.

For the Pre-Amp, when AC voltage $\dot{V}$ is applied to input G, the AC voltage difference between $\rm O_1$ and $\rm O_2$ is denoted as $\dot{V}_{\rm op}$. $A_{\rm vP} = \dot{V}_{\rm op}/\dot{V}$ is the voltage gain of the Pre-Amp. Since the gain-bandwidth-product of the CNRS-HEMT is $g_{\rm m}/[2\pi(C_{\rm gs}+C_{\rm gd})] \approx 1$ GHz, the bandwidth of the Pre-Amp is more than 30 MHz. In $\max\{g_{\rm m}/(2\pi C_{\rm S}), 1/(2\pi R_{\rm S} C_{\rm S}), 1/(2\pi R_{\rm S} C_2)\} << f \leq 3$ MHz (i.e. 167 Hz $<< f \leq 3$ MHz with the parameters listed in Table 1),

$$A_{\rm vP} \approx -g_{\rm m} R_{\rm d}, \tag{2.1}$$

chinaXiv:202212.00178v3

Table 1: Parameters of all components of CryoSTM-TIA circuit

CNRS-HEMTs C-H			
Gate–source resistance R_A			>10 TΩ
Transconductance g_m			40 mS
Channel conductance g_d			1 mS
Gate–source capacitance C_{gs}			5 pF
Gate–drain capacitance C_{gd}			1 pF
Drain–source voltage V_{ds}			100 mV
Drain–source current I_{ds}			1 mA
$\overline{e_H^2}$ $((nV)^2/Hz)$		10 kHz	0.25
		100 kHz	0.07
$\overline{i_H^2}$ $((fA)^2/Hz)$		10 kHz	0.1
		100 kHz	1
Pre-Amp			
R_S	100 ± 5 Ω	C_S	0.1 mF
R_H	200 ± 5 Ω	R_L	1 kΩ
R_{p1}	10 Ω	R_{p2}	10 ± 10 Ω
C_1& C_2	10 μF		
T_1 & T_2	BJT BFT93 [16]	R_b	347 ± 1 Ω
R_t	20 kΩ	V_{Pp}	+12 V
Post-Amp with THS4021 as Rear-OPA			
a_{a0}	97.5 dB	f_b	14.5 kHz
C_a	1.5 pF	R_a	1 MΩ
R_f	330 kΩ	C_i	100 pF
Supply voltages V_{Rp}, V_{Rn}			+15, -15 V
Feedback network			
R_F	1 GΩ	C_F	∼ 0.3 pF
R_k	100 kΩ	C_k	∼ 0.2 pF
C_c	3 nF		
Signal source circuit			
R_J	≥1 MΩ	C_I	∼ 0.5 pF

Note: ± indicates the variable resistance range. Without specification, the default value after ± is 0.

where $R_d = R_L/(1 + R_L g_d)$. i.e., $A_{vP} \approx -20$ in 167 Hz$<<$ $f \leq 3$ MHz. The input capacitance of the Pre-Amp is

$$C_A = C_{gs} + (1 - A_{vP})C_{gd}. \tag{2.2}$$

i.e., $C_A \approx 26$ pF in 167 Hz$<<$ $f \leq 3$ MHz. The input resistance of the Pre-Amp R_A is the gate-source resistance of C-H, and $R_A > 10$ TΩ, so it can be considered as infinity.

The constant-current source part of the Pre-Amp shown in the dashed box (a2) in Fig.1 is the same as in Ref.[3]. For a given resistance R_b, there is almost no fluctuation for the current I_{sour} generated by the constant-current source, even though the voltage V_{Pp} of the positive voltage source fluctuates greatly, which ensures the stability of the operating point for C-H.

2.2 Design of Post-Amp and composition of Inv-Amp

In Fig.1, the Post-Amp circuit in the dashed box (b) is the same in structure as that in Ref.[3]. There is a commercial operational amplifier (OPA) in the circuit, called as Rear-

chinaXiv:202212.00178v3

OPA, which is the OPA with high gain-bandwidth-product, such as THS4021, OPA657, and LMH6624, etc. R_a and C_a are the input resistance and capacitance of Rear-OPA respectively. The feedback resistor R_f is connected to output O of Rear-OPA and its inverting input. R_f is 330 kΩ, and it placed in the cryogenic zone. The Post-Amp also contains two cables that connect the non-inverting input and inverting input of the Rear-OPA to outputs O_1 and O_2 of the Pre-Amp respectively. The capacitance of the two cables is C_{i1} and C_{i2} respectively, and $C_{i1} = C_{i2} = C_i \approx 100$ pF. The Rear-OPA in this work is THS4021 [17], and $C_i >> C_a$. The Post-Amp parameters are listed in Table 1.

Cascade the Pre-Amp and Post-Amp to form the Inv-Amp. For the AC signal, the voltage gain of the Inv-Amp is $a_A = a_A(f)$. $a_A(f)$ can be expressed as

$$a_A = A_{vP} A_{vR}. \tag{2.3}$$

By the nodal analysis method, a_A can be obtained. And then, with A_{vP} expressed by Eq.(2.1), A_{vR} can be obtained by Eq.(2.3). In $\max\{g_m/(2\pi C_S), 1/(2\pi R_S C_S), 1/(2\pi R_S C_2)\} << f \le 3$ MHz (i.e. 167 Hz $<< f \le 3$ MHz with the parameters listed in Table 1),

$$A_{vR} \approx \frac{R_f}{R_{HL}} \cdot \frac{1 + j2\pi f R_{HL} C_i}{1 + j2\pi f R_d C_i} \cdot \frac{1}{1 + \frac{R_f}{a_a R_{HL}} + j2\pi f \frac{R_f C_i}{a_a}}, \tag{2.4}$$

where $R_{HL} = R_H R_L/(R_H + R_L)$ and a_a is the voltage gain of the Rear-OPA. In this work, $R_f >> R_{HL}$ and $R_a >> R_{HL}$. And, a_a can be approximately expressed as $a_a = a_{a0}/(1 + jf/f_b)$ in (0, 40 MHz] for THS4021.

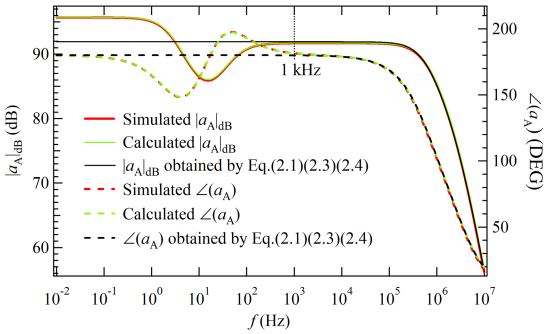

Figure 2: The Inv-Amp voltage gain $a_A(f)$. The solid curves are the curves of $|a_A(f)|_{dB}$, and the dashed curves are the curves of $\angle(a_A(f))$. The red curves are the TINA-TI simulation results, the green curves are the calculated results with the nodal analysis method, and the black curves are the calculated results by Eqs.(2.1), (2.3), and (2.4) in Article.

With the parameters in Table 1, the Inv-Amp performances can be simulated by TINA-TI [18]. Fig.2 show the curves of $|a_A(f)|_{dB}$ and $\angle(a_A(f))$ simulated by TINA-TI. By the nodal analysis method, $a_A(f)$ is calculated by the equations established with all components listed in Table 1 [19], which is also shown in Fig.2. The curves of $|a_A(f)|_{dB}$ and $\angle(a_A(f))$ calculated by the nodal analysis method are identical with the simulated ones respectively. $|a_A(f)|_{dB}$ and $\angle(a_A(f))$ are also calculated by Eqs.(2.1), (2.3), and (2.4), and the calculated curves in Fig.2 are almost identical with the simulated ones respectively in [1 kHz, 10 MHz], which verifies the correctness of Eqs.(2.1),(2.3), and (2.4).

chinaXiv:202212.00178v3

2.3 Frequency compensation of feedback loop

In order to increase the bandwidth of the CryoSTM-TIA, for the high feedback resistor $R_{\rm F}$ with parasitic capacitance $C_{\rm F}$, frequency compensation must be used in the feedback loop [1, 20]. In Fig.1, the compensated feedback network is shown in the dashed box (c). $R_{\rm F}$ is placed as near as possible to C-H for reducing the capacitance between the gate G of C-H and Ground. Taking $C_{\rm c}$ equalto $kC_{\rm F}$, where k is above 10^3, adjust $R_{\rm k}$ equalto $R_{\rm F}/k$, realizing $R_{\rm k}C_{\rm c} = R_{\rm F}C_{\rm F}$. The output voltage of the TIA as $\dot{V}_{\rm o}$ generates the current $\dot{I}_{\rm F}$ flowing to input G of the TIA, so

$$Z_{\rm F}(f) = \frac{\dot{V}_{\rm o}}{\dot{I}_{\rm F}} \approx \frac{R_{\rm k}+R_{\rm F}}{1+j2\pi f R_{\rm k}C_{\rm k}} \approx \frac{R_{\rm F}}{1+j2\pi f R_{\rm k}C_{\rm k}},$$

where $C_{\rm k}$ is the parasitic capacitance of $R_{\rm k}$ [1, 3, 20]. $Z_{\rm F}(f)$ can be considered as the impedance of the feedback network. In Ref.[20], it has been achievedin experiments to broaden the bandwidth of the feedback network with the very high feedback resistor $R_{\rm F}$ of 10 GΩ to MHz. In (0, 1 MHz], with the parameters listed in Table 1, $|Z_{\rm F}(f)| \approx R_{\rm F}/|1+j2\pi f R_{\rm k}C_{\rm k}| > R_{\rm F}/1.008$ and $|Z_{\rm F}(f)| \le R_{\rm F}$, so it can be considered that $Z_{\rm F}(f)$ is equal to $R_{\rm F}$.

2.4 Circuit stability of the proposed CryoSTM-TIA

In Fig.1, the signal source circuit is shown in the dashed box (d), and its parameters are shown in Table 1. The differential resistance of the tip-sample tunnel junction (TJ) is $R_{\rm J}$, which is limited to no less than $10^{-3}R_{\rm F}$ in this design. The capacitance of TJ is $C_{\rm J}$, which is in parallel with $R_{\rm J}$. And, $C_{\rm J}$ is estimated as several fF [3]. $C = C_{\rm A}+C_{\rm I}+C_{\rm J}$ in this work. $C_{\rm J}$ is at least two orders of magnitude less than $C_{\rm A}+C_{\rm I}$, so it can be ignored in C and $C \approx C_{\rm A}+C_{\rm I}$. The DC bias & modulated signal voltage source is denoted as BMS, which provides the DC bias $V_{\rm i}$ and sinusoidal modulated signal voltage $\dot{V}_{\rm i}$ for the CryoSTM-TIA. In the following simulation, $C_{\rm I}$ is always taken as 0.5 pF. The TIA connects the signal source circuit to form the CryoSTM-TIA. According to the parameters in Table 1, the performances of the CryoSTM-TIA can be simulated by TINA-TI.

The loop gain $T_{\rm L}$ of the proposed CryoSTM-TIA [21] is

$$T_{\rm L}(f) = -a_{\rm A}(f)\beta(f) = -a_{\rm A}(f)/[1/\beta(f)],$$

in which $\beta(f)$ is the feedback factor, and its reciprocal is,

$$1/\beta(f) \approx 1 + Z_{\rm F}[1/R_{\rm J} + 1/R_{\rm A} + j2\pi f(C_{\rm A}+C_{\rm I})]. \tag{2.5}$$

By Eq.(2.5), $|1/\beta(f)|$ and $\angle(1/\beta(f))$ can be calculated. Fig.3(a) shows the calculated results of $|1/\beta(f)|_{\rm dB}$ and $\angle(1/\beta(f))$ with $R_{\rm J} = +\infty$, and Fig.3(b) shows those with $R_{\rm J} = 1$ MΩ. $|a_{\rm A}|_{\rm dB}$ and $\angle(a_{\rm A})$ are also shown in Fig.3. Both figures show $|T_{\rm L}|_{\rm dB} = |a_{\rm A}|_{\rm dB} - |1/\beta(f)|_{\rm dB} \le -10$ dB in $f \ge 512$ kHz and $\angle(T_{\rm L}) = \angle(-a_{\rm A}) - \angle(1/\beta) = \angle(a_{\rm A}) - 180° - \angle(1/\beta) > -138°$ in $f \le 512$ kHz. Therefore, the CryoSTM-TIA is stable with gain margin more than 10 dB and phase margin more than 42°.

chinaXiv:202212.00178v3

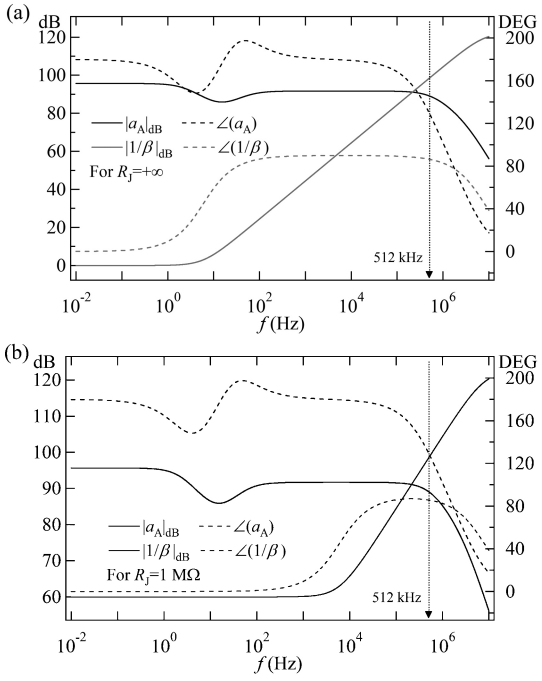

Figure 3: TINA-TI simulation results for the voltage gain Inv-Amp a_A, and $1/\beta(f)$ (a) with $R_J = +\infty$, (b) with $R_J = 1$ MΩ. Both figures show $|T_L|_{dB} = |a_A|_{dB} - |1/\beta(f)|_{dB} \leq -10$ dB in $f \geq 512$ kHz and $\angle(T_L) = \angle(-a_A) - \angle(1/\beta) = \angle(a_A) - 180° - \angle(1/\beta) > -138°$ in $f < 512$ kHz. Hence, the CryoSTM-TIA is stable enough.

2.5 Voltage gain and transimpedance gain of the proposed CryoSTM-TIA

With the compensated feedback network mentioned in Sect.2.3, it can be considered that Z_F is equal to R_F in (0, 1 MHz]. Considering the TJ capacitance C_J, the TJ impedance should be $Z_J = R_J/(1 + j2\pi f R_J C_J)$. And, $C \approx C_A + C_I$. As the AC input voltage $\dot{V}_i$ is applied by BMS, the output voltage of the CryoSTM-TIA is $\dot{V}_o$, and the voltage gain of the CryoSTM-TIA is $A_v = \dot{V}_o/\dot{V}_i$. In (0, 1 MHz], by the nodal analysis method, A_v is

$$A_v \approx -\frac{R_F}{Z_J} \cdot \frac{1}{1 - \frac{1}{a_A} - \frac{R_F}{a_A R_J} - \frac{R_F}{a_A R_A} - j2\pi f \frac{R_F(C_A+C_I)}{a_A}}. \tag{2.6}$$

Setting $\dot{V}_i = 0$ and applying a sinusoidal current source $\dot{I}_i$ in parallel with TJ, the output voltage $\dot{V}_o$ is generated at the output of the CryoSTM-TIA. $A_i = \dot{V}_o/\dot{I}_i$ is called as the transimpedance gain of the CryoSTM-TIA. In (0, 1 MHz], A_i is

$$A_i \approx -\frac{R_F}{1 - \frac{1}{a_A} - \frac{R_F}{a_A R_J} - \frac{R_F}{a_A R_A} - j2\pi f \frac{R_F(C_A+C_I)}{a_A}}. \tag{2.7}$$

Disconnecting the TIA with the signal source circuit, and applying a sinusoidal current source $\dot{I}_{iT}$ into the input of the TIA, the output voltage $\dot{V}_{oT}$ is generated at the output of the TIA. $A_{iT} = \dot{V}_{oT}/\dot{I}_{iT}$ is called as the transimpedance gain of the TIA. In (0, 1 MHz],

A_{iT} is

$$A_{\mathrm{iT}} = -\frac{R_{\mathrm{F}}}{1 - \frac{1}{a_{\mathrm{A}}} - \frac{R_{\mathrm{F}}}{a_{\mathrm{A}} R_{\mathrm{A}}} - j2\pi f \frac{R_{\mathrm{F}} C_{\mathrm{A}}}{a_{\mathrm{A}}}}, \tag{2.8}$$

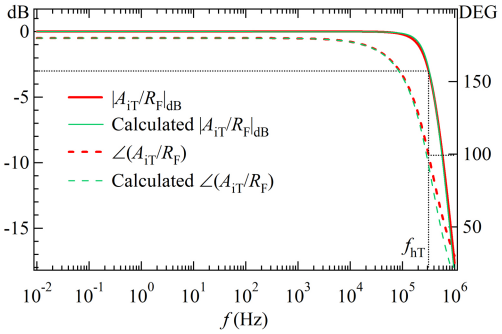

Figure 4: TINA-TI simulation results for $A_{\mathrm{iT}}/R_{\mathrm{F}}$, A_{iT} is the transimpedance gain of the TIA in the proposed CryoSTM-TIA. $|A_{\mathrm{iT}}(f_{\mathrm{hT}})/R_{\mathrm{F}}|_{\mathrm{dB}} = -3$ dB and $\angle(A_{\mathrm{iT}}(f_{\mathrm{hT}})/R_{\mathrm{F}}) = 99^{\circ}$ at $f_{\mathrm{hT}} = 320$ kHz.

In Fig.4, $|A_{\mathrm{iT}}/R_{\mathrm{F}}|_{\mathrm{dB}}$ and $\angle(A_{\mathrm{iT}}/R_{\mathrm{F}})$ calculated by Eq.(2.8) with the parameters in Table 1 is identical with their TINA-TI simulation results in [1 kHz, 1 MHz], which verifies the correctness of Eq.(2.8) for A_{iT}. The upper cut-off frequency of $A_{\mathrm{iT}}(f)/R_{\mathrm{F}}$, i.e. its -3 dB frequency is $f_{\mathrm{hT}} = 320$ kHz. Comparing Eq.(2.7) with Eq.(2.8), as $C_{\mathrm{A}} + C_{\mathrm{I}} + C_{\mathrm{J}} \approx C_{\mathrm{A}} + C_{\mathrm{I}} \approx C_{\mathrm{A}}$ and $R_{\mathrm{J}} \geq 10^{-3} R_{\mathrm{F}}$, the upper cut-off frequency of the CryoSTM-TIA is approximately equal to f_{hT}.

2.6 Transient response of the proposed CryoSTM-TIA

The simulation results for the transient response of the proposed CryoSTM-TIA are shown in Supplemental file 2 [22]. For the CryoSTM-TIA, the time taken from adding the input step signal voltage to the output response stably within a certain error is called transient response time t_{r}. For the simulations, a resistor with a constant resistance R_0 is instead of the tip-sample junction. When $R_0 \geq 30$ MΩ, for 0.1% error, $t_{\mathrm{r}} < 5$ μs. When 5 MΩ $\leq R_0 < 30$ MΩ, for 1% error, $t_{\mathrm{r}} < 5$ μs. When 1 MΩ $\leq R_0 < 5$ MΩ, for 3% error, $t_{\mathrm{r}} < 5$ μs.

3 Inherent noise of the proposed CryoSTM-TIA

For the circuit of the proposed CryoSTM-TIA shown in Fig.1, the differential equivalent circuit with all noise sources is used to calculate its equivalent input noise. The details for the noise calculations are shown in Supplemental file 3 [24].

3.1 Equivalent input voltage noise and equivalent input current noise of Inv-Amp

The equivalent input noise voltage and equivalent input noise current of C-H are denoted as e_{H} and i_{H} respectively. The resistors R_1, R_2, and R_{f} are in the cryogenic zone of 4.2 K,

chinaXiv:202212.00178v3

chinaXiv:202212.00178v3

and their noises in $f > 1$ kHz are thermal noise, which can be neglected [3]. The thermal noise voltage of the resistor $R_{\rm H}$ is $e_{\rm RH}$. The equivalent input noise voltage and equivalent input noise current of the Rear-OPA are denoted as $e_{\rm a}$ and $i_{\rm a}$ respectively. These noise sources are independent. The equivalent input noise voltage and equivalent input noise current of the Inv-Amp are denoted as $e_{\rm A}$ and $i_{\rm A}$ respectively. By the nodal analysis method and Wiener-Sinchin theorem, ignoring the minor terms, it is obtained that

$$\overline{e_{\rm A}^2} = \overline{e_{\rm H}^2} + \frac{R_{\rm HL}^2}{R_{\rm H}^2}\frac{\overline{e_{\rm RH}^2}}{A_{\rm vP}^2} + \frac{\overline{e_{\rm a}^2}}{A_{\rm vP}^2} + \left(1+\frac{R_{\rm HL}}{R_{\rm d}}\right)^2 \frac{\overline{i_{\rm a}^2}}{g_{\rm m}^2}, \tag{3.1}$$

$$\overline{i_{\rm A}^2} = \overline{i_{\rm H}^2} + (2\pi f)^2 \frac{C_{\rm A}^2}{A_{\rm vP}^2}\left(\frac{R_{\rm HL}^2}{R_{\rm H}^2}\overline{e_{\rm RH}^2} + \overline{e_{\rm a}^2}\right) + (2\pi f)^2 \left(C_{\rm gs}+C_{\rm gd}+\frac{R_{\rm HL}}{R_{\rm d}}C_{\rm A}\right)^2 \frac{\overline{i_{\rm a}^2}}{g_{\rm m}^2}, \tag{3.2}$$

$$\begin{aligned}\overline{e_{\rm A}i_{\rm A}^*} =& (\overline{i_{\rm A}e_{\rm A}^*})^* = -j2\pi f \frac{C_{\rm A}}{A_{\rm vP}^2}\left(\frac{R_{\rm HL}^2}{R_{\rm H}^2}\overline{e_{\rm RH}^2} + \overline{e_{\rm a}^2}\right) \\ & - j2\pi f \left(C_{\rm gs}+C_{\rm gd}+\frac{R_{\rm HL}}{R_{\rm d}}C_{\rm A}\right)\left(1+\frac{R_{\rm HL}}{R_{\rm d}}\right)\frac{\overline{i_{\rm a}^2}}{g_{\rm m}^2}.\end{aligned} \tag{3.3}$$

According to the parameters listed in Table 1, for the Inv-Amp in this work, $\overline{e_{\rm A}^2} = 0.27$ $({\rm nV})^2/{\rm Hz}$ and $\overline{i_{\rm A}^2} = 0.13$ $({\rm fA})^2/{\rm Hz}$ at $f = 10$ kHz, and $\overline{e_{\rm A}^2} = 0.08$ $({\rm nV})^2/{\rm Hz}$ and $\overline{i_{\rm A}^2} = 2.7$ $({\rm fA})^2/{\rm Hz}$ at $f = 100$ kHz. For the Macro-OPA in Ref.[3], $\overline{e_{\rm A}^2} = 0.5$ $({\rm nV})^2/{\rm Hz}$ and $\overline{i_{\rm A}^2} = 0.8$ $({\rm fA})^2/{\rm Hz}$ at $f = 10$ kHz, and $\overline{e_{\rm A}^2} = 0.14$ $({\rm nV})^2/{\rm Hz}$ and $\overline{i_{\rm A}^2} = 20$ $({\rm fA})^2/{\rm Hz}$ at $f = 100$ kHz. The resistor $R_{\rm H}$ in the Inv-Amp in this work replaces the transistor H2 in the Macro-OPA in Ref.[3]. The noise generated by $R_{\rm H}$ is 2 orders of magnitude smaller than that generated by H2 in the Macro-OPA in Ref.[3], i.e. $\overline{e_{\rm RH}^2} << A_{\rm vP}^2\overline{e_{\rm H}^2}$. Therefore, the equivalent input noises of the Inv-Amp in this work are much lower than those of the Macro-OPA in Ref.[3].

In $f \geq 10$ kHz, $\overline{e_{\rm a}^2} = 2.25$ $({\rm nV})^2/{\rm Hz}$ and $\overline{i_{\rm a}^2} = 4$ $({\rm pA})^2/{\rm Hz}$ [17]. In Eqs.(3.1), (3.2), and (3.3), $\overline{e_{\rm RH}^2}R_{\rm HL}^2/R_{\rm H}^2$ is one order of magnitude smaller than $\overline{e_{\rm a}^2}$. In Eq.(3.1), $(1+R_{\rm HL}/R_{\rm d})^2\,\overline{i_{\rm a}^2}/g_{\rm m}^2$ is 2 orders of magnitude smaller than $\overline{e_{\rm H}^2}$. In Eq.(3.2), $(C_{\rm gs}+C_{\rm gd}+C_{\rm A}R_{\rm HL}/R_{\rm d})^2\,\overline{i_{\rm a}^2}/g_{\rm m}^2$ is one order of magnitude smaller than $C_{\rm A}^2\overline{e_{\rm a}^2}/A_{\rm vP}^2$. In Eq.(3.3), $(C_{\rm gs}+C_{\rm gd}+C_{\rm A}R_{\rm HL}/R_{\rm d})\,(1+R_{\rm HL}/R_{\rm d})\,\overline{i_{\rm a}^2}/g_{\rm m}^2$ is one order of magnitude smaller than $C_{\rm A}\overline{e_{\rm a}^2}/A_{\rm vP}^2$. Further ignoring the minor terms in Eqs.(3.1), (3.2), and (3.3),

$$\overline{e_{\rm A}^2} = \overline{e_{\rm H}^2} + \overline{e_{\rm a}^2}/A_{\rm vP}^2, \tag{3.4}$$

$$\overline{i_{\rm A}^2} = \overline{i_{\rm H}^2} + (2\pi f)^2 C_{\rm A}^2\overline{e_{\rm a}^2}/A_{\rm vP}^2, \tag{3.5}$$

$$\overline{e_{\rm A}i_{\rm A}^*} = (\overline{i_{\rm A}e_{\rm A}^*})^* = -j2\pi f C_{\rm A}\overline{e_{\rm a}^2}/A_{\rm vP}^2. \tag{3.6}$$

3.2 Equivalent input current noise of the proposed CryoSTM-TIA

The equivalent input noise current PSD of the proposed CryoSTM-TIA is obtained as

$$\begin{aligned}\overline{i_{\rm in}^2} =& \overline{i_{\rm A}^2} + 4k_{\rm B}T/R_{\rm F} + \left[1/R_{\rm J}^2 + 1/R_{\rm F}^2 + (2\pi f)^2 C_{\rm IJ}^2\right]\overline{e_{\rm A}^2} \\ & + (1/R_{\rm J} + j2\pi f C_{\rm IJ})\left(\overline{e_{\rm A}i_{\rm A}^*} + \overline{e_{\rm A}^2}/R_{\rm F}\right) \\ & + (1/R_{\rm J} - j2\pi f C_{\rm IJ})\left(\overline{i_{\rm A}e_{\rm A}^*} + \overline{e_{\rm A}^2}/R_{\rm F}\right),\end{aligned} \tag{3.7}$$

where $C_{IJ} = C_I + C_J$ [3, 23, 24]. Putting Eqs.(3.4), (3.5), and (3.6) into Eq.(3.7),

$$\begin{aligned}\overline{i_{in}^2} =& \overline{i_H^2} + 4k_BT/R_F + (1/R_J + 1/R_F)^2 \left(\overline{e_H^2} + \overline{e_a^2}/A_{vP}^2\right) \\ &+ (2\pi f)^2 \left(C_{IJ}^2\overline{e_H^2} + C^2\overline{e_a^2}/A_{vP}^2\right), \end{aligned} \tag{3.8}$$

i.e.

$$\overline{i_{in}^2} = \overline{i_A^2} + 4k_BT/R_F + (1/R_J + 1/R_F)^2\,\overline{e_A^2} + \overline{i_{CIJ}^2}, \tag{3.9}$$

where $\overline{i_{CIJ}^2} = (2\pi f)^2(C_{IJ}^2\overline{e_A^2} + 2C_AC_{IJ}\overline{e_a^2}/A_{vP}^2)$.

For the proposed CryoSTM-TIA, $R_F = 1$ GΩ, $C_A = 26$ pF, $C_I = 0.5$ pF, and $C_J = 10$ fF. R_F and TJ are in the cryogenic zone at 4.2K. As $R_J = 1$ MΩ, $\overline{i_{in}^2}$ and its four components are listed in Table 2. The noise components of the CryoSTM-TIA in Ref.[3] are also shown in Table 2. The CryoSTM-TIA proposed in this work has an equivalent input noise current PSD of 0.6 $(\text{fA})^2$/Hz at 10 kHz and 3 $(\text{fA})^2$/Hz at 100 kHz, which is much lower than that in Ref.[3].

Table 2: Noise components of CryoSTM-TIAs

Pre-Amp type	Single HEMT Amp		Pre-Amp in Ref.[3]	
f (kHz)	10	100	10	100
$\overline{e_A^2}$ $((\text{nV})^2/\text{Hz})$	0.27	0.08	0.5	0.14
Unit for the following terms is $(\text{fA})^2/\text{Hz}$				
$\overline{i_A^2}$	0.13	2.7	0.8	20
$4k_BT/R_F$	0.2	0.2	0.2	0.2
$\overline{i_{CIJ}^2}$	0.0013	0.06	0.03	0.7
$(\frac{1}{R_J} + \frac{1}{R_F})^2\overline{e_A^2}$	0.26	0.08	0.5	0.14
$\overline{i_{in}^2}$ as total	0.6	3	1.5	21

According to the work on the noise mechanism of the CNRS-HEMT [5], "bias-cooling method" can be used to control the density of the frozen DX^- centers in the doping area in the HEMT. This unique method, by which the in-situ modification of the HEMT structure is realized, can be used to reduce the noise generated by the HEMT. By cooling the HEMT with the positive gate-source voltage, more electrons in the HEMT are frozen into the DX^- centers. At low temperatures, the absolute of the gate-source voltage required to maintain the HEMT at the ideal operating point is reduced, so that the gate leakage current is reduced, and thus the low frequency noises generated by the gate leakage current is reduced [5]. By the means, the inherent noise of the CryoSTM-TIA can be reduced. Moreover, if the HEMT used for the CryoSTM-TIA is not CNRS-HEMT, or its noise performances are not as good as those listed in Table 1, it can be remedied by "bias-cooling method". This approach is very convenient for cases with only a single HEMT in the Pre-Amp.

4 Operating state adjustment and DC tunneling current measurements

For the CryoSTM-TIA in Fig.1, along with the circuit parameters listed in Table 1, its operating state can be adjusted as follows. (1) Disconnect the Pre-Amp from the Post-Amp and ground the input of the Pre-Amp, i.e. gate G of C-H. Adjust R_{p2} to $R_{p2} = R_{p1}$.

chinaXiv:202212.00178v3

chinaXiv:202212.00178v3

Adjust the constant-current source to generate current as $I_{sour} = 2$ mA. Adjust R_{s1} and R_{h1} to achieve C-H at the ideal operating point ($V_{ds} = 100$ mV, $I_{ds} = 1$ mA) and the potentials at O_1 and O_2 equal. That is to say, R_{s1} and R_{h1} are adjusted to realize $R_H = R_S + V_{ds}/I_{ds} = R_S + 100\ \Omega$. (2) Cascade the Pre-Amp and Post-Amp to form the Inv-Amp, and input G is still grounded. By then, the DC output voltage V_{om} of the Inv-Amp is usually not 0. V_{om} is induced by the input offset voltage of the Rear-OPA [17], its input bias currents and input offset current, and the common-mode DC voltages on the the inputs of the Rear-OPA. Adjust R_{h1} and R_{p2} to achieve the current through R_{p2} back to 1 mA and $V_{om} = 0$. Therefore, C-H is also at the ideal operating point. (3) Connect output O and input G of the Inv-Amp with the feedback network and disconnect input G from ground, to form the TIA. Input G is still not connected with the signal source circuit, so the potential of input G and output O of the Inv-Amp is still 0, since the input resistance of the transistor C-H R_A can be considered as infinity. In the feedback network, $R_F + R_k \approx R_F = 1$ GΩ. (4) Connect the signal source circuit to the TIA, to form the CryoSTM-TIA.

When $f \to 0$, $a_A \to a_{A0}$, and a_{A0} is the DC voltage gain of the Inv-Amp. $|a_{A0}|_{dB} \approx (g_m R_f/g_d R_H)_{dB} \approx 96.4$ dB, which is consistent with the simulation result $|a_{A0}|_{dB} = 95.6$ dB shown in Fig.2. As the DC bias V_i is applied by BMS, the DC resistance of TJ is R, and the potential at input G is V_G, and the output voltage of the CryoSTM-TIA is V_o. Obviously, $a_{A0}V_G = V_o$, and $(V_i - V_G)/R = (V_G - V_o)/R_F$. The DC bias on TJ is $V = V_i - V_G$, and the DC tunneling current $I = (V_i - V_G)/R$. I_s as an approximate value of I is

$$I_s = -V_o/R_F. \tag{4.1}$$

And, the relative error is obtained as

$$Er = |I_s - I|/|I| = 1/(1 - a_{A0}).$$

As $|a_{A0}|_{dB} \approx 96$ dB, $Er < 20$ ppm, consistent with the simulation results [25]. Since $a_{A0}V_G = V_o$, the DC bias on TJ is

$$V = V_i - V_o/a_{A0}. \tag{4.2}$$

By Eq.(4.1), $V_o = -R_F I_s \approx -R_F I = -R_F V/R$. By Eq.(4.2), $V_i \approx V - R_F V/(R a_{A0})$. As the minimum of R_J is not less than 1 MΩ, $R \geq 1$ MΩ, so $|R_F/(R a_{A0}| \leq 1/60$. Thus, $V \approx V_i$. With the measured V_o, $I \approx I_s$ and $V \approx V_i$ can be obtained. Therefore, the scanning tunneling current spectra $I = I(V)$ ($V \in [V_L, V_H]$) can be obtained, where V_L and V_H are the lower limit and upper limit voltages for the measurements respectively.

It should be noted that the Pre-Amp in this work is not a differential structure, so there is no function for it to counteract the influences of the temperature drift as that for the differential structure. The drift of V_{om} can be considered as the amplification of the drift of the Inv-Amp input offset voltage V_{OS}, where $V_{om} = a_{A0}V_{OS}$. The estimated drift of $|V_{OS}|$ is about 0.5 mV/°C [26]. The power of the constant-current source is about 24 mW. The well-designed temperature Control System based on the TEC devices [27] can be used to control the temperature fluctuations of the constant-current source within 0.0002 °C [28] and those of Rear-OPA within 0.1 °C, so the fluctuations of V_{OS} within 150 nV is guaranteed, i.e. the TIA output fluctuations within 150 nV [3].

chinaXiv:202212.00178v3

5 Applications for the proposed CryoSTM-TIA in spectra measurements

For most applications, the modulus of the transimpedance gain of the CryoSTM-TIA $|A_{\rm i}(f)|$ should be measured firstly. $A_{\rm i}(f)$ is expressed as Eq.(2.7). Since $|a_{\rm A}(f)|_{\rm dB} > 90$ dB in [1 kHz, 300 kHz] as shown in Fig.2, when $R_{\rm J} \geq 10^{-3} R_{\rm F}$, $|A_{\rm i}(f)|$ in [1 kHz, 300 kHz] can be approximately expressed as

$$|A_{\rm i}(f)| = R_{\rm F}/|1 - j2\pi f R_{\rm F}(C_{\rm A} + C_{\rm I})/a_{\rm A}(f)|. \tag{5.1}$$

How to measure it has been described in Ref.[3].

5.1 Measurements of scanning tunneling differential conductance spectra by the proposed CryoSTM-TIA

The differential conductance of TJ $G_{\rm J} = 1/R_{\rm J}$ is the function of the voltage V applied to TJ. As the frequency f of the modulated signal voltage $\dot{V}_{\rm i}$ provided by BMS is low enough, such as $f < 1$ kHz, by Eq.(2.6),

$$A_{\rm v} \approx \frac{R_{\rm F}}{R_{\rm J}(V)} \cdot \frac{1}{1 - \frac{R_{\rm F}}{a_{\rm A}(f) R_{\rm J}(V)}}.$$

Therefore, $R_{\rm J}(V) \approx [1/A_{\rm v} + 1/a_{\rm A}(f)]\, R_{\rm F}$. When the measured $|A_{\rm v}| \leq 1000$, $R_{\rm J}(V) \approx R_{\rm F}/|A_{\rm v}|$, since $|a_{\rm A}(f)|_{\rm dB} \geq 85$ dB in $f \leq 300$ kHz as shown in Fig.2. With the measured $|A_{\rm v}| = |\dot{V}_{\rm o}|/|\dot{V}_{\rm i}|$, the differential conductance spectra $G_{\rm J}(V) = 1/R_{\rm J}(V)$ ($V \in [V_{\rm L}, V_{\rm H}]$) can be obtained.

Increasing the frequency f of the modulated signal can speed up the scanning tunneling differential conductance spectra measurements. In [1 kHz, 300 kHz], as $R_{\rm J} \geq 1$ MΩ, by Eq.(2.6),

$$|A_{\rm v}(f)| \approx \frac{1}{|Z_{\rm J}(f)|} \cdot \frac{R_{\rm F}}{|1 - j2\pi f R_{\rm F}(C_{\rm A} + C_{\rm I})/a_{\rm A}(f)|}.$$

Therefore, $1/|Z_{\rm J}(f)| \approx |A_{\rm v}(f)|/|A_{\rm i}(f)|$, where $|A_{\rm i}(f)|$ is shown by Eq.(5.1). And, $|A_{\rm v}(f)|$ and $|A_{\rm i}(f)|$ can be measured. $1/|Z_{\rm J}(f)| = \sqrt{1/R_{\rm J}^2 + (2\pi f C_{\rm J})^2}$ can be obtained. Selecting two different frequencies f_1 and f_2 in [1 kHz, 300 kHz], $|Z_{\rm J}(f_1)|$ and $|Z_{\rm J}(f_2)|$ are obtained. $R_{\rm J}$ and $C_{\rm J}$ can be solved out from the measured $|Z_{\rm J}(f_1)|$ and $|Z_{\rm J}(f_2)|$.

Since the inherent noise of the CryoSTM-TIA is very small, the amplitude of the modulated signal voltage $\dot{V}_{\rm i}$ can be very small (≤ 10 μV), so that the energy resolution for STS is much improved.

5.2 Measurements of scanning tunneling shot noise spectra by the proposed CryoSTM-TIA

The measurement method for the tunneling shot noise spectra by the proposed CryoSTM-TIA is basically the same as that introduced by Ref.[3], and it is only briefly described here.

chinaXiv:202212.00178v3

Before approaching the tip to the sample in the CryoSTM, $R_{\rm J}$ can be considered as infinity and $C_{\rm J}$ as 0. In this case, the output noise voltage PSD of the CryoSTM-TIA $S_{\rm su}(f)$ can be measured, and the equivalent input noise current PSD $\overline{i_{\rm i}^2}(f)$ is

$$\overline{i_{\rm i}^2}(f) = S_{\rm su}(f)/|A_{\rm i}(f)|^2, \tag{5.2}$$

where $|A_{\rm i}(f)|$ is obtained by Eq.(5.1).

To measure the scanning tunneling shot noise spectra (STSNS) of a quantum system by the CryoSTM-TIA, the distance between the tip and sample is adjusted, and the interval $[V_{\rm L},\ V_{\rm H}]$ is selected, so that the shot noise measurements at $V \in D_{\rm V} = \{V|\ V_{\rm L} \le V \le V_{\rm H}, G_{\rm J}(V) < 1\ \mu{\rm S}\}$ are needed to study the physical properties of the quantum system [3]. In $D_{\rm V}$, the output noise voltage PSD $S_{\rm sum}(f,V)$ can be measured. The tunneling noise current PSD is denoted as $S_{\rm I}(f,V)$. The equivalent input noise current PSD of the CryoSTM-TIA is the function of $R_{\rm J}$, so it is the function of V and denoted as $\overline{i_{\rm in}^2}(f,V)$. For $S_{\rm sum}(f,V)$,

$$S_{\rm sum}(f,V) = \left[S_{\rm I}(f,V) + \overline{i_{\rm in}^2}(f,V)\right] \cdot |A_{\rm i}(f)|^2. \tag{5.3}$$

With Eq.(5.2) and (5.3), it is obtained that

$$S_{\rm I}(f,V) = \frac{S_{\rm sum}(f,V) - S_{\rm su}(f)}{|A_{\rm i}(f)|^2} - [\overline{i_{\rm in}^2}(f,V) - \overline{i_{\rm i}^2}(f)]. \tag{5.4}$$

From Eq.(3.9),

$$\overline{i_{\rm i}^2}(f) = \overline{i_{\rm A}^2} + \frac{4k_{\rm B}T}{R_{\rm F}} + \frac{\overline{e_{\rm A}^2}}{R_{\rm F}^2} + (2\pi f)^2\left(C_{\rm I}^2\overline{e_{\rm A}^2} + 2C_{\rm A}C_{\rm I}\frac{\overline{e_{\rm a}^2}}{A_{\rm vP}^2}\right).$$

And, $\overline{i_{\rm in}^2}(f,V)$ is composed by the four parts as shown in Eq.(3.9). According to Table 2, $\delta(f,V)$ as the difference between $\overline{i_{\rm in}^2}(f,V)$ and $\overline{i_{\rm i}^2}(f)$ is smaller than 0.3 $({\rm fA})^2/{\rm Hz}$ in [10 kHz, 100 kHz) and 0.1 $({\rm fA})^2/{\rm Hz}$ in[100 kHz, 300 kHz]. $\delta(f,V)$ can be neglected compared with $S_{\rm I}(f,V)$, so long as the minimum of $G_{\rm J}(V)$ $(V \in D_{\rm V})$ is not too small. Therefore, $S_{\rm I}(f,V)$ can be obtained as

$$S_{\rm I}(f,V) \approx \frac{S_{\rm sum}(f,V) - S_{\rm su}(f)}{|A_{\rm i}(f)|^2}, \tag{5.5}$$

by the measured $S_{\rm sum}(f,V)$, $S_{\rm su}(f)$, and $|A_{\rm i}(f)|$. And then, the SNTNS $S_{\rm Is}(I) = 2Fe|I|$ can be extracted from $S_{\rm I}(f,V)$. Here, $I = I(V)$ $(V \in D_{\rm V})$, and I is the DC tunneling current as the bias V is applied.

Compared with the CryoSTM-TIA in Ref.[3], the CryoSTM-TIA proposed in this work has the same bandwidth and transimpedance gain, but its inherent noise is much lower. The inherent noise of the CryoTM-TIA in this work is only 3 $({\rm fA})^2/{\rm Hz}$ at 100 kHz and its $\delta(f,V) < 0.1$ $({\rm fA})^2/{\rm Hz}$ at 100 kHz, while that of the apparatus in Ref.[3] is 21 $({\rm fA})^2/{\rm Hz}$ at 100 kHz and $\delta(f,V) < 0.28$ $({\rm fA})^2/{\rm Hz}$ at 100 kHz. Therefore, as investigating novel quantum states of various quantum systems, the measurements performed with the apparatus proposed in this work is more accurate.

For example, as investigating the existence of MBS in a magnetic flux vortex of the iron superconductor in CryoSTM [4], the tunnel junction resistance must be large enough,

since the occurrence of incoherent Andreev reflection can be ruled out by weak tunnel coupling conditions [29]. In Ref.[4], the tunneling current I is quite low (see Fig.3(a) in Ref.[4] and Fig.S1(a) and (b) in its supplemental file). As the tunnel junction bias V is 0.3 mV, I is only tens of pA, and the corresponding shot noise may only be only a few $(\text{fA})^2/\text{Hz}$. For the shot noise measurements in the system in Ref.[4], it is obvious that the CryoSTM-TIA proposed in this work is much more effective and accurate than that in Ref.[3].

6 Conclusions

In this work, a design of transimpedance amplifier (TIA) for cryogenic scanning tunneling microscope (CryoSTM) is presented. The TIA connected with the tip-sample component in CryoSTM is called as CryoSTM-TIA. The CryoSTM-TIA in this work has transimpedance gain of 1 GΩ and bandwidth more than 300 kHz, and its equivalent input noise current PSD is only 3 $(\text{fA})^2/\text{Hz}$ at 100 kHz. In this CryoSTM-TIA, a single CNRS-HEMT Pre-Amp is instead of the differential Pre-Amp consisting of a pair of CNRS-HEMTs in Ref.[3]. The difficulty of matching the identical HEMTs is avoided. And, due to the reduction of a noisy HEMT, the apparatus inherent noise is only 1/7 of that in Ref.[3]. Furthermore, the inherent noise of the single HEMT in the circuit can be in-situ reduced by "bias-cooling method". With this apparatus, the fast high-energy-resolution scanning tunneling spectra measurements can be performed and the very low tunneling shot noise of quantum systems can be measured at the atomic scale. This apparatus can be applied to investigate novel physical properties of various quantum systems, such as detecting the existence of Majorana bound states in the topological quantum systems.

chinaXiv:202212.00178v3

Acknowledgment

This work is supported by Open Research Fund Program of the State Key Laboratory of Low-Dimensional Quantum Physics (Grant No. KF202212). I acknowledge stimulating discussions with Prof. Fang-Hao Liang of Math School in Shandong Univ and Prof. Xing Liang of Math School in USTC.

Declaration of competing interest

The author declares that they have no known competing financial interests or personal relationships that could have appeared to influence the work reported in this paper.

References

[1] C.J. Chen, Introduction to scanning tunneling microscopy, Oxford Univ. Press, (1993).

[2] J.F. Ge, M. Ovadia, and J.E. Hoffman, Achieving low noise in scanning tunneling spectroscopy, Rev. Sci. Instrum., 90 (2019) 101401, https://doi.org/10.1063/1.5111989.

chinaXiv:202212.00178v3

[3] Y.X. Liang, Low-noise large-bandwidth tansimpedance amplifier for measuring scanning tunneling shot noise spectra in cryogenic STM and its applications, Ultramicroscopy, 234, (2022) 13466, https://doi.org/10.1016/j.ultramic.2022.113466.

[4] D.F. Wang, L.Y. Kong, P. Fan, H. Chen, S.Y. Zhu, W.Y. Liu, L. Cao, Y.J. Sun, S.X. Du, J. Schneeloch, R.D. Zhong, G.D. Gu, L. Fu, H. Ding, and H.J. Gao, Evidence for Majorana bound states in an iron-based superconductor, Science, 362 (2018) 333, https://doi.org/10.1126/science.aao1797.

[5] Y.X. Liang, Q. Dong, M.C. Cheng, U. Gennser, A. Cavanna, and Y. Jin, Insight into low frequency noise induced by gate leakage current in AlGaAsGaAs high electron mobility transistors at 4.2 K, Appl. Phys. Lett., 99 (2011) 113505. https://doi.org/10.1063/1.3637054.

[6] Y. Jin, Q. Dong, A. Cavanna, U. Gennser, L. Couraud, and C. Ulysse, Ultra-low noise HEMTs for deep cryogenic low-frequency and highimpedance readout electronics, 12th IEEE International Conference on Solid-State and Integrated Circuit Technology (ICSICT) (2014).

[7] K.M. Bastiaans, D. Cho, T. Benschop, I. Battisti, Y. Huang, M.S. Golden, Q. Dong, Y. Jin, J. Zaanen, and M.P. Allan, Charge trapping and super-Poissonian noise centres in a cuprate superconductor, Nat. Phys., 14 (2018) 1183. https://doi.org/10.1038/s41567-018-0300-z.

[8] F. Massee, Y.K. Huang, M.S. Golden, and M. Aprili, Noisy defects in the high-T_c superconductor $Bi_2Sr_2CaCu_2O_{8+x}$, Nat. Commun., 10 (2019) 544. https://doi.org/10.1038/s41467-019-08518-1.

[9] C.J. Bolech and E. Demler, Observing majorana bound states in p-wave superconductors: using noise measurements in tunneling experiments, Phys. Rev. Lett. 98, (2007) 237002, https://doi.org/10.1103/PhysRevLett.98.237002.

[10] A. Golub and B. Horovitz, Shot noise in a Majorana fermion chain, Phys. Rev. B 83, (2011)153415, https://doi.org/10.1103/PhysRevB.83.153415.

[11] H. Soller and A. Komnik, Charge transfer statistics of transport through Majorana bound states, Physica E 63, (2014) 99, https://doi.org/10.1016/j.physe.2014.05.020.

[12] C.W.J. Beenakker and D.O. Oriekhov, Shot noise distinguishes Majorana fermions from vortices injected in the edge mode of a chiral p-wave superconductor, SciPost Phys. 9, (2020), 080, https://doi.org/ 10.21468/SciPostPhys.9.5.080.

[13] K.M. Bastiaans, D. Cho, D. Chatzopoulos, M. Leeuwenhoek, C. Koks, and M.P. Allan, Imaging doubled shot noise in a Josephson scanning tunneling microscope, Phys. Rev. B, 100 (2019) 104506. https://doi.org/10.1103/PhysRevB.100.104506.

[14] K.M. Bastiaans, D. Chatzopoulos, J.F. Ge, D. Cho, W.O. Tromp, J.M. van Ruitenbeek, M.H. Fischer, P.J. de Visser, D.J. Thoen, E.F.C. Driessen, T.M. Klapwijk, and M.P. Allan, Direct evidence for Cooper pairing without a spectral gap in a disordered superconductor above T_c, Science 374 (2021) 608. https://doi.org/10.1126/science.abe3987.

chinaXiv:202212.00178v3

[15] S. Cocklin and D.K. Morr, Scanning tunneling shot-noise spectroscopy in Kondo systems, Phys. Rev. B, 100 (2019) 125146, https://doi.org/10.1103/PhysRevB.100.125146.

[16] Data sheet of BFT93 BJT, https://www.nxp.com.cn/docs/en/datasheet/BFT93 CNV.pdf.

[17] Data sheet of THS4021 OPA, https://www.ti.com/lit/ds/symlink/ths4021.pdf.

[18] TINA-TI is SPICE-based analog simulation program produced by Texas Instruments Inc., https://www.ti.com/tool/TINA-TI.

[19] Supplemental file 1. Please ask Author for it by email.

[20] B. Michel, L. Novotny, and U. Dürig, Ultramicroscopy 42-44, 1647 (1992).

[21] S. Franco, Design with Operational Amplifiers and Analog Integrated Circuits,McGraw-Hill Companies, Inc., (2002).

[22] Supplemental file 2. Please ask Author for it by email.

[23] A. van der Ziel, Noise in solid state devices and circuits, Wiley-Inter-Science, New York, (1986).

[24] Supplemental file 3. Please ask Author for it by email.

[25] Supplemental file 4. Please ask Author for it by email.

[26] Supplemental file 5. Please ask Author for it by email.

[27] A suitable TEC device, https://datasheets.maximintegrated.com/en/ds/MAX1978-MAX1979.pdf.

[28] W. Zhang, Z.L. Li, P. Guo, and J.Y. Zhao, Design of precise temperature control system for saturated absorption Frequency stabilization of DFB Laser, Semicond. Optoelectron., 41 (2020) 560, https://doi.org/10.16818/j.issn1001-5868.2020.04.021.

[29] L.Y. Kong and H. Ding, Emergent vortex Majorana zero mode in iron-based superconductors, Acta. Phys. Sin., 69 (2020) 110301, https://doi.org/10.7498/aps.69.20200717.